JOURNAL OF APPLIED ELECTROCHEMISTRY 25 (1995) 533–542

# Heat generation during pulse operation of prototype aluminium electrolytic capacitors

R. S. ALWITT

*Boundary Technologies, Inc., 366 Lexington Drive, Buffalo Grove, IL 60089, USA*

S. G. PARLER, JR*

*Cornell Dubilier Marketing, Inc., PO Box 128, Pickens, SC 29671, USA*

Received 4 March 1994; revised 1 August 1994

Measurements were made of heat generation in aluminium electrolytic capacitor 'sandwiches' operating under pulse charge and discharge. With commercial anode foils the fraction of input power dissipated as heat in the dielectric is proportional to the *DF* of the oxide dielectric. There is also a dependence on the applied voltage that is thought to be due to frictional losses arising from expansion and relaxation of the oxide in the pulsed field. This field dependence is specific to the commercial etched aluminium foils and is absent when the oxide dielectric is grown on smooth substrate, indicating a dependence of the stresses in the oxide on the etch structure. The oxide degrades under isothermal pulse operation at 60° C, with both *DF* and heat generation increasing proportionally. Oxide 'reformation' brings these properties back to their initial values, or lower, and stabilizes the dielectric during subsequent pulse operation. An amorphous anodic oxide dielectric deposited at room temperature on commercial etched foils had different characteristics. The fractional heat dissipation was equal to the lowest observed with the commercial oxides, but was independent of oxide *DF*. Long term isothermal pulsing produced only slight degradation of the oxide properties.

## 1. Introduction

Aluminium electrolytic capacitors are favoured for pulse discharge applications because of their high energy density. However, rapid pulse discharge results in unacceptable temperature rise in the capacitor. As part of a program to develop capacitors which could be pulsed at more rapid rate [1], determinations were made of power dissipation in capacitors, calculated from the capacitor temperature rise and thermal properties. It was found that about 10% of the input power was dissipated, a significantly larger quantity than would be calculated from a.c. bridge measurements of capacitor dissipation factor (*DF*), e.g., at 120 Hz. Moreover, the power dissipated did not exhibit the expected dependence on the square of voltage, but rather had a $V^3$ dependence. As a first step to understand these observations, we studied this behaviour under more easily controlled, and hence better defined, conditions.

Calorimetric measurements were made of heat generation in prototype electrolytic capacitors operated under pulse conditions. These capacitors were small coupons of anode and cathode foil separated by electrolyte-impregnated spacer paper, and held between glass microscope slides. We focus here on those properties of the anode foil that are important to heat generation. Behaviour was observed that can partially account for the 'excess' heat generation and superquadratic voltage dependence observed during capacitor operation, but there is not a complete correspondence between the capacitor 'sandwiches' and commercial capacitors. Additional experiments are needed to achieve a more precise understanding of the dissipation process.

The basic elements of the capacitor are the anode foil that is coated with an oxide dielectric, an organic electrolyte solution to provide electrical continuity, a porous spacer to hold the electrolyte, and a cathode foil to serve as a current collector. The anode foil capacitance is close to that of a parallel plate capacitor, with the metal/oxide interface as the positive plate and the oxide/electrolyte interface as the negative plate. The cathode foil generally has a thin air-formed oxide on its surface that acts like a dielectric.

The device capacitance is that of the anode and cathode foils in series. The usual practice is to select a cathode foil with a capacitance much greater than that of the anode, in order to realize a device capacitance close to that of the anode foil. A related requirement for cathode foil used in pulse discharge applications is to be capable of electrostatically storing the charge released from the anode foil. If the cathode plate area is insufficient, then some anodic oxide will form on the cathode during each discharge pulse. This reduces device capacitance, causes strong local heating and gas generation at the anode, and results in rapid failure.

* Current address: Maven Capacitor Corporation, PO Box 90, Liberty SC 29657, USA.

0021-891X 

The anode and cathode foils are electrochemically etched to increase surface area. The etch structure of the anode foils used in these experiments is a high density ($> 10^7$ cm$^{-2}$) of etch tunnels about 1 $\mu$m in diameter that penetrate into the body of the foil to depths up to 50 $\mu$m [2]. The etched foil is electrochemically treated to form a barrier oxide dielectric film over the etched surface, with the film thickness proportional to the oxide formation voltage. The oxide structure may be amorphous, crystalline, or a mixture of the two, depending upon particular process conditions [3, 4]. Foil manufacturers vary the process details to produce foils with high capacitance in a certain voltage range, and with stable dielectric properties.

The capacitor circuit elements measured with an a.c. bridge are the series capacitance and the equivalent series resistance (ESR). The ESR is the sum of the contribution from the electrolyte-impregnated spacer ($R_{sp}$), an ohmic resistance, and the resistance of the oxide dielectric ($R_{ox}$). The oxide resistance depends upon the frequency, and on a smooth substrate $R_{ox}$ is inversely proportional to frequency. When using etched foil as substrate, the distribution of oxide capacitance and electrolyte resistance over the rough surface affects the frequency response. As frequency increases the interior of this electrode tends to be 'tuned out'. This increases the effective oxide resistance, and a plot of ESR against the period (Hz$^{-1}$) exhibits some downward curvature. This behaviour is shown in Fig. 1 for several commercial capacitors. The dashed lines connect the ESR values at the highest and lowest measuring frequencies, 1000 and 120 Hz. Data points at intermediate frequencies lie slightly above these lines.

When an alternating voltage is applied to a capacitor, the resulting alternating current consists of two components: an out of phase current which charges the dielectric, and an in-phase component which causes dissipation of energy as heat. The series circuit and phasor diagram are shown in Fig. 2. The capacitor dissipation factor ($DF$) is the ratio of the loss voltage to ideal capacitor voltage.

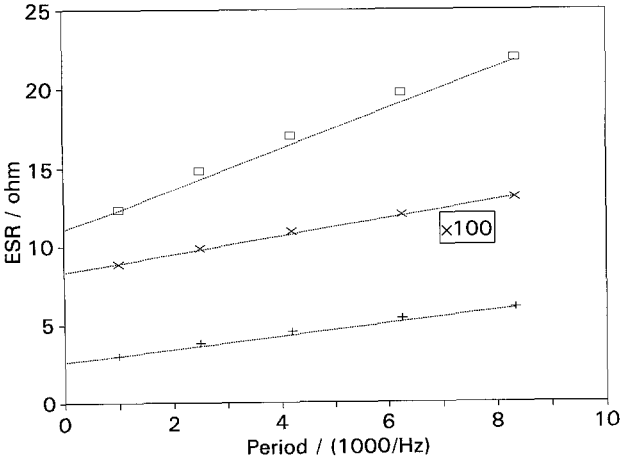


Fig. 1. Frequency dependence of ESR for three commercial capacitors. (□) 3.3 $\mu$F 160 WF, (+) 10 $\mu$F 350 WF and (×) 470 $\mu$F 200 WV. Note scale change for 470 $\mu$F capacitor.

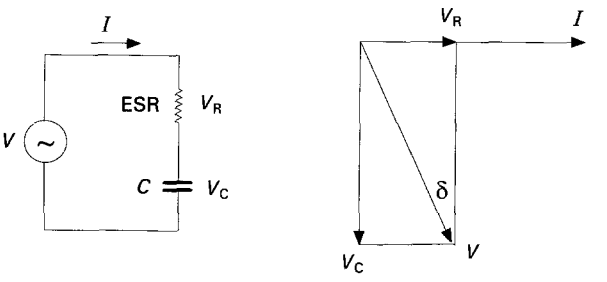


Fig. 2. Electrolytic capacitor equivalent series circuit and phasor diagram.

The $DF$ is measured by the response to a small a.c. sinusoidal signal with an amplitude of order $10^{-1}$ V; the field in the oxide during measurement is 10–100 V cm$^{-1}$. In contrast, during pulse operation, a high voltage capacitor is operated at several hundred volts, with the field in the oxide dielectric greater than $5 \times 10^6$ V cm$^{-1}$ and the pulse shape is not sinusoidal. It is not obvious that the loss processes under these conditions will be limited to those occurring during the bridge measurement.

Application of a step voltage across a capacitor and series resistor causes an increase in voltage across the capacitor accompanied by a decay of current in the circuit. Capacitor discharge through the series resistor produces a decay of both current and voltage across the capacitor. The circuit time constant, $\tau$, is the time in which the current (voltage) decays by 1/e. The time constant is governed primarily by the series $RC$ circuit elements, but is also influenced by particular properties of the dielectric (cf. [5]).

When used in a pulse power application, the capacitor charge time is usually relatively long compared with the discharge time. In the present experiments the charge and discharge periods are equal, and the average input power is calculated over one cycle of charge and discharge. In that case,

$$W_{in} = \frac{1}{2T}\int_0^T I(t)V(t)\,dt \qquad (1)$$

where $I(t)$ and $V(t)$ are the time dependent current and capacitor voltage, and $T$ is the charge time.

## 2. Experimental details

### 2.1. *Capacitor specimen*

A test capacitor consisted of strips of foil and spacer paper sandwiched between glass microscope slides. The foils were flag-shaped coupons with 2.54 cm × 3.81 cm body and 6.4 mm wide handle. The spacer paper was wetted with electrolyte prior to assembly. The usual structure was a central anode foil with a layer of spacer and cathode foil on either side, but in a few cases multiple stacks were used. Small bar clamps provided uniform pressure along the sandwich. Electrical contact to each foil electrode was made by pressing the end of a 0.25 mm diam. aluminium wire firmly against the coupon handle. The

contact area was protected with silicone grease from inadvertent exposure to electrolyte.

After assembly, 'ageing' is necessary to form oxide on foil edges and repair any damage that may have been caused to the dielectric during handling. This step was done for time intervals from several hours to overnight, and either at room temperature or 85° C. The particular conditions had no discernible effect on test results. A.c. bridge measurements of sandwich $C$ and $DF$ were made at 120 and 1000 Hz at the start and end of each experimental run. These data were used to estimate $R_{sp}$. The charging current transient was measured at the start of each experiment.

The etched anode foils used throughout the program were a sampling of commercially available materials, and none were known to have been designed specifically for use in pulse applications. The foils were obtained mostly from two major suppliers and were characterized by differences in degree of surface enhancement by etching, and different oxide formation voltages ($V_f$). The oxide dielectrics were formed using proprietary processes, specific to each supplier, of which we have limited knowledge. We infer that there are differences in the formation processes because of differences in oxide properties found in laboratory tests.

The etched cathode foil, spacer paper, and electrolyte were commercially available materials. The cathode foil was selected to have sufficient plate area to reversibly charge and discharge during pulse operation. The electrolyte was an ethylene glycol formulation and the spacer was a low density Manila paper. These materials were selected to minimize ohmic contribution. Temperature rise during pulse operation occurs even with capacitors designed with minimal ohmic resistance, and it is well established that ohmic heating is not a critical factor contributing to failure.

Some experiments were done with foil specimens on which the oxide was grown in our laboratory. Conditions were selected to simulate certain commercial practices, and one low temperature process was used that produced a fully amorphous dielectric layer. Laboratory formations were also done on smooth aluminium substrates in order to evaluate the effect of the foil etch structure.

### 2.2. *Electrical circuitry*

Constant voltage pulses were generated using a signal generator to operate a transistor switch that was on the output of a d.c. power supply. The sandwich capacitor was charged through resistor $R_1$ and discharged through resistor $R_2$. These resistors were always matched, so with $R_1 = R_2$, values of $T$ and $\tau$ for charging were equal to those for discharge. Values of $R$ and $T$ were chosen so $2\tau < T < 3\tau$; this resulted in a small truncation of the charging voltage, but larger values for $T$ reduced the level of heat generation. The time-dependent current, $I(t)$, was determined from the voltage drop across a 0.1 Ω resistor, which was measured with an oscilloscope. The capacitor voltage was calculated as the difference between the applied pulse voltage and the voltage drop across the load resistor, $V(t) = V_p - I(t)R_1$.

### 2.3. *Calorimeter*

The calorimeter consisted of a 100 ml Dewar flask with a head made of rigid foam insulation material, through which passed the electrical connections and thermocouple wire. The top edge of the capacitor sandwich fit snugly into a slot in the bottom of the head, and was suspended in this way within the calorimeter body. The calorimeter was filled with 75 ml of ethylene glycol, which brought the liquid level to the top of the foil body, but below the zone of electrical contact. To minimize heat exchange with the surroundings, the calorimeter was immersed in a constant temperature water bath set at the initial temperature of the test. The bath was placed on a magnetic stirrer, and a slowly rotating stir bar in the calorimeter maintained uniform temperature. The calorimeter was calibrated from the rate of temperature rise produced by a fixed current through a known resistance immersed in the electrolyte. The calibration factor was checked periodically. It did not change perceptibly over a set of runs (1–2 days), but some slow changes were apparent over longer times (weeks). Over the course of this work it was in the range 0.20 to 0.22° C $min^{-1}$ $W^{-1}$. Calculations were always made using the most recent calibration factor.

Temperature was measured with a thermocouple suspended in the calorimeter. It was connected to an Omega series DP85/86 temperature indicator whose potential (mV) output was recorded against time using a strip chart recorder. The temperature increase during a test was always linear with time, and from this slope and the calorimeter calibration factor the rate of heat generation ($W_{cal}$) was calculated. Measurement time at one condition was typically 1 h and no more than 3 h; the time was varied in order to obtain a temperature rise of 2–3° C, independent of the rate of heat generation. Temperatures were measured with an accuracy of 0.1° C.

### 2.4. *Fraction of input energy converted to heat*

The input power, $W_{in}$, is calculated from Equation 1. The $I$–$t$ table for a charge transient was put into a spreadsheet program and $W_{in}$ was calculated by numerical integration. The fraction of power (or energy) dissipated as heat in the calorimeter is $W_{cal}/W_{in}$. We subtract from this the ohmic loss ($W_{sp}$) in the spacer/electrolyte. For one charge and one discharge period the ohmic power is,

$$W_{sp}/W_{in} = 2\gamma(R_{sp}/R_L) \qquad (2)$$

In Equation 2, $\gamma = (1 - e^{-\beta} + e^{-2\beta})/(1 - 2e^{-\beta} + e^{-2\beta})$ and $\beta = T/\tau$. This function varies slowly with $\beta$; for

$\beta = 2$ or 3, $\gamma = 1.19$ or 1.06, respectively. $R_L$ is the load resistor, $R_1$ or $R_2$.

A value for $R_{sp}$ was calculated from the a.c. bridge measurements at 120 and 1000 Hz. A linear dependence of $R_{ox}$ on the period was assumed, and the intercept at zero period was taken as $R_{sp}$. This calculation is illustrated by the dashed lines in Fig. 1; it results in a value for $R_{sp}$ that may be less than the true value. The offset depends on the particular foil and electrolyte, but for several high voltage capacitors was estimated to be in the range 5–10%.

The fraction of power dissipated as heat in the oxide dielectric is

$$W_{ox}/W_{in} = W_{cal}/W_{in} - W_{sp}/W_{in} \quad (3)$$

This quantity is compared with the oxide *DF*, which is obtained from the measured capacitor *DF* after subtracting the ohmic contribution from spacer/electrolyte:

$$DF_{ox} = DF_{cap} - 2\pi f R_{sp} C_f \quad (4)$$

where $C_f$ is the a.c. capacitance measured at the frequency $f$. Our calculations are for $f = 120$ Hz.

Because of the approximation in $R_{sp}$, the ohmic terms on the right hand side of Equations 3 and 4 are too small by 5–10%. The selection of materials and experimental conditions limited the contribution of ohmic dissipation to no more than 1/3 of total heat generated, and it was usually 15–20% of the total. Thus, the net effect of this systematic error is to calculate values for $W_{ox}/W_{in}$ and $DF_{ox}$ that are too large by no more than 5%. This is too small an error to affect the interpretation of the results. Most importantly, since $W_{ox}/W_{in}$ and $DF_{ox}$ are equally affected by this approximation, it has no effect when we compare them.

### 2.5. *Isothermal pulse procedure*

After initial a.c. bridge and calorimetric measurements, a sandwich capacitor was placed in an ethylene glycol bath in a constant temperature environment, either kept near 20° C or 60° C. Voltage pulses were applied for a period of time, usually over several days. Bridge measurements were made periodically *in situ*, and at the end of the pulse period the sandwich was removed for a final calorimetric measurement.

## 3. Results

### 3.1. *Anodic oxide on smooth Al substrates*

Initial measurements were made using smooth aluminium foils on which anodic oxide had been formed in the laboratory to 275 V. Oxides were grown on aluminium using three different formation conditions. Two were high temperature processes typical of those used in commercial practice; they produced a dielectric layer that contained both amorphous and crystalline oxide. The other was a room temperature process known to produce only amorphous oxide. It consisted of a sequence of an initial anodization that deposited a porous oxide followed by a second anodization that deposited barrier oxide within and under the porous oxide [6]. Properties of the oxides and general information about their formation are summarized in Table 1. The oxide labelled 'phos' was typically formed in a phosphate solution at voltages no higher than 300 V. At the upper end of this range the oxide film may be partially crystalline [7]. The process sequence used to make the oxide labelled 'comp' is typical of that used to make most high voltage anode foils, although process details and bath chemistry vary widely. It is referred to as a composite oxide [3, 8], and tends to have a fine-grained crystalline structure although some amorphous oxide may be present.

*Table 1. Smooth foil sandwiches*
275 $V_f$ Oxide Dielectrics, 2 anode foils/sandwich

| *Type* | *Process* | *C*/μF | $DF_{ox}$ | *Oxide thickness*/nm | $R_1$/Ω |
|---|---|---|---|---|---|
| Phos | (1) | 0.785 | 0.016 | 360 | 1000 |
| Comp | (2) | 1.039 | 0.022 | 275 | 800 |
| Amorph | (3) | 0.858 | 0.020 | 330 | 950 |

(1) Form in 0.5 g $dm^{-3}$ $NH_4H_2PO_4$ at 85° C, 15 mA per specimen. Hold 6 min at 275 V, or until current drops to 1 mA.
(2) Immerse specimen in boiling water for 3 min to grow hydrous oxide. Form in 5 g $dm^{-3}$ ammonium adipate + 5 g $dm^{-3}$ ammonium pentaborate at 85° C, 15 mA per specimen. Hold at 275 V for total time of 6.7 min. Follow with two depolarization and two reformation steps.
(3) Form porous oxide in 80 g $dm^{-3}$ oxalic acid dihydrate at 20° C, 200 mA for 4 min. Then form barrier oxide in 0.5 M $H_3BO_3$ + 0.05 M $Na_2B_4O_7$ at 20° C, 10 mA per specimen. Hold at 275 V for 10 min. More details are found in [6].

Calorimetry measurements were made on sandwiches containing two anode foils in the stack, at pulse voltages of 150, 200, 250 V and a pulse rate of 212 Hz. The values of $R_L$ used with each sandwich are listed in Table 1. The rate of heat generation ($W_{cal}$) against pulse voltage is shown in Fig. 3. The lines are drawn with slope = 2. There is scatter of the data about these lines, but no slope significantly different from two would better describe the results. Ohmic heating is proportional to $V^2$, so subtraction

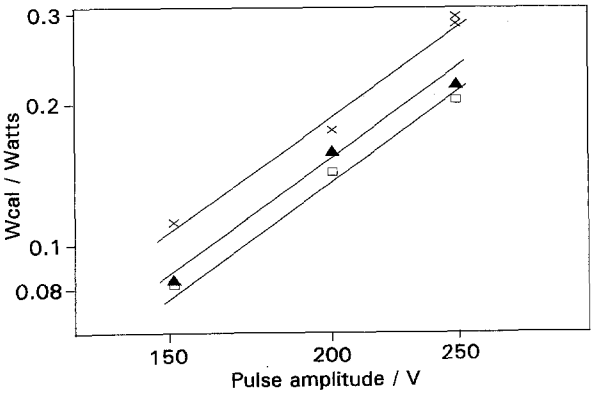


Fig. 3. Logarithmic plot of rate of heat generation in calorimeter against pulse voltage for several oxide types on smooth aluminium substrates; pulse frequency: 212 Hz. See Table 1 for description of oxides and $R_L$ values. Oxides: (□) phos; (×) comp; (▲) amorph.

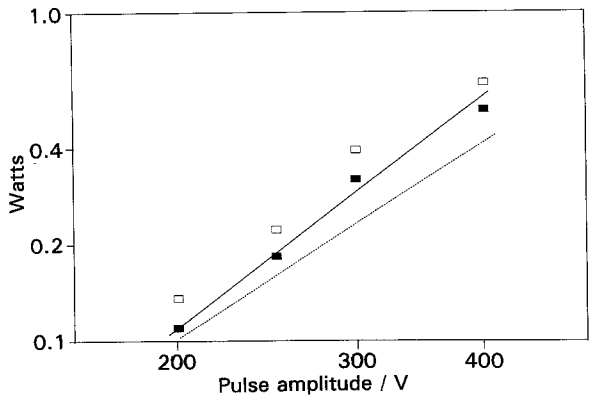


Fig. 4. Logarithmic plot of heat generation against pulse voltage for 9 $\mu$F 400 WV capacitor; pulse frequency = 10 Hz. (□) $W_{cal}$; (■) $W_{ox}$. Slope of solid line: 2.30; slope of dashed line: 2.00.

of $W_{sp}$ to obtain $W_{ox}$ does not change the $V^2$ dependence of heat generation. The fraction of input power dissipated as heat in the dielectric, $W_{ox}/W_{in}$, was similar for the two sandwiches containing commercial-type aluminium oxide dielectrics. The values are 0.036 for process 1 and 0.039 for process 2. The amorphous oxide dissipated only 0.027 of input power.

### 3.2. *Miniature electrolytic capacitor*

One experiment was done with a commercial miniature aluminium electrolytic capacitor rated at 400 V and with a capacitance of 9.3 $\mu$F at 120 Hz. Calorimetric measurements were made at a 10 Hz pulse rate and with $R_L = 1000\,\Omega$. The spacer resistance was found to be 2.9 Ω. The voltage dependence of $W_{cal}$ and $W_{ox}$ is shown in Fig. 4. The solid line has a slope of 2.3. At 200 V, $W_{ox}/W_{in} = 0.050$, and at 400 V that ratio is 0.055.

### 3.3. *Anodic aluminium oxide on commercial etched foils*

The voltage dependence of $W_{cal}$ was measured for the commercial anode foils described in Table 2, which also lists the test conditions. Foils B and E are from one supplier and foils A, C and D are from another supplier. The oxides labelled 300A and 300M are both formed to 300 V on the same type etched foil, but different composite oxide type formation processes were used. The first two specimens listed are etched foils with lab-formed oxides. The fraction of crystalline oxide in these dielectrics was calculated

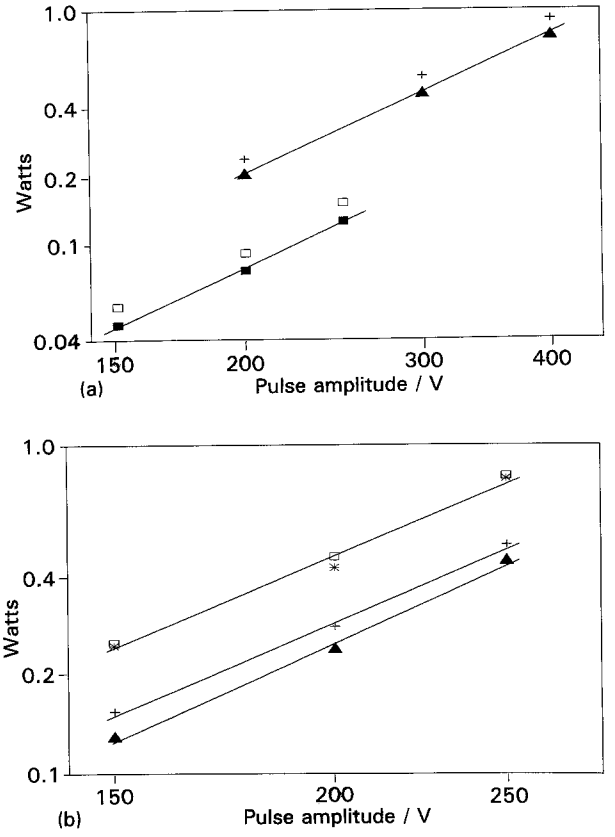


Fig. 5. (a) Logarithmic plot of heat generation against pulse voltage for commercial foils. See Table 2 for description of foils and circuit parameters. (□) foil C350, $W_{cal}$; (■) foil C350, $W_{ox}$; (+) foil D550, $W_{cal}$; (▲) foil D550, $W_{ox}$. (b) Logarithmic plot of heat generation ($W_{cal}$) against pulse voltage for commercial foils. Voltage dependence of heat generation of commercial foils. See Table 2 for description of foils and circuit parameters. (*) foil B300A; (□) foil B300M; (▲) foil B275phos; (+) foil A275amorph.

from the weight fraction found to be insoluble in a hot phosphoric acid-chromic oxide solution [2, 9], and these estimates are shown in Table 2.

The dependence of $W_{cal}$ and $W_{ox}$ on $V_f$ is shown in Fig. 5(a) for two of the commercial foils. For each of these foils $W_{cal}$ and $W_{ox}$ exhibit the same voltage dependence, and both the lines have slopes of 2.0. The dependence of $W_{cal}$ on pulse voltage for four other foils listed in Table 2 is shown in Fig. 5(b). The lines through these data have slopes as large as 2.4. There is no obvious dependence of the exponent on foil or oxide type, e.g., the lab-formed amorphous oxide on etched foil had $n = 2.4$, in the same range as for the commercial foils. It may be significant that the two foils with $n = 2$ also were the foils with the lowest

*Table 2. Etched foil sandwiches*

| *Code* | $V_f$ | *Oxide* | *Cryst*/% | *Foils* | $C/\mu F$ | *Pulse*/Hz | $R_L/\Omega$ | $n$* |
|---|---|---|---|---|---|---|---|---|
| B | 275 | phos | – | 1 | 6.44 | 50 | 500 | 2.43 |
| A | 275 | amorph | 0 | 1 | 6.68 | 50 | 500 | 2.43 |
| B | 300A | commerc. | >90 | 1 | 8.97 | 50 | 360 | 2.34 |
| B | 300M | commerc. | >90 | 1 | 9.53 | 50 | 350 | 2.34 |
| C | 350 | commerc. | ~50 | 1 | 2.24 | 50 | 1450 | 2.00 |
| D | 550 | commerc. | >90 | 1 | 3.38 | 10 | 1000 | 2.02 |
| E | 550 | commerc. | >90 | 2 | 8.49 | 1 | 500 | – |

* Slope in Fig. 5.

*Table 3. Summary of calorimetric results*

| *Foil* | $V_f$/V | *Oxide* | *Cap*/μF | $DF_{ox}$ | $W_{ox}/W_{in}$ | *n* | $V/V_f$ | *norm* $W_{ox}/W_{in}$ |
|---|---|---|---|---|---|---|---|---|
| C | 350 | commerc. | 2.24 | 0.0194 | 0.0364 | 2 | 0.714 | 0.0364 |
| C | 350 | commerc. | 2.24 | 0.018 | 0.0373 | 2 | 0.429 | 0.0373 |
| B | 300 | commerc. | 8.97 | 0.0197 | 0.0456 | 2.34 | 0.833 | 0.0383 |
| B | 300 | commerc. | 9.53 | 0.0173 | 0.0406 | 2.34 | 0.833 | 0.0341 |
| C | 450 | commerc. | 1.74 | 0.0134 | 0.0270 | 2 | 0.556 | 0.0270 |
| A | 255 | commerc. | 8.88 | 0.0286 | 0.0536 | 2.43 | 0.784 | 0.0442 |
| B | 300 | commerc. | 9.53 | 0.0235 | 0.0512 | 2.34 | 0.833 | 0.0430 |
| C | 250 | commerc. | 4.01 | 0.0219 | 0.0406 | 2 | 1.000 | 0.0406 |
| C | 550 | commerc. | 1.43 | 0.0158 | 0.0495 | 2 | 0.455 | 0.0495 |
| C | 650 | commerc. | 1.13 | 0.0166 | 0.0534 | 2 | 0.385 | 0.0534 |
| C | 450 | commerc. | 1.76 | 0.015 | 0.0351 | 2 | 0.556 | 0.0351 |
| D | 650 | commerc. | 2.21 | 0.0272 | 0.0491 | 2 | 0.385 | 0.0491 |
| D | 550 | commerc. | 2.98 | 0.0207 | 0.0432 | 2 | 0.455 | 0.0432 |
| D | 450 | commerc. | 4.26 | 0.0228 | 0.0424 | 2 | 0.556 | 0.0424 |
| A | 500 | amorph. | 3.17 | 0.0159 | 0.0220 | 2 | 0.500 | 0.0220 |
| A | 600 | amorph. | 2.46 | 0.0122 | 0.0220 | 2 | 0.417 | 0.0220 |
| A | 650 | amorph. | 2.35 | 0.0104 | 0.0270 | 2 | 0.385 | 0.0270 |
| A | 275 | amorph. | 6.68 | 0.0225 | 0.0302 | 2.43 | 0.909 | 0.0234 |
| A | 325 | amorph. | 5.67 | 0.0185 | 0.0227 | 2.43 | 0.615 | 0.0208 |
| A | 400 | amorph. | 4.59 | 0.021 | 0.0250 | 2.43 | 0.500 | 0.0250 |
|  | 400 | capacitor | 9.31 | 0.0176 | 0.0500 | 2.32 | 0.500 | 0.0500 |
| smooth | 275 | phos. | 0.79 | 0.0163 | 0.0358 | 2 | 0.909 | 0.0358 |
| smooth | 275 | comp. | 1.04 | 0.0223 | 0.0387 | 2 | 0.909 | 0.0387 |
| smooth | 275 | amorph. | 0.86 | 0.0197 | 0.0271 | 2 | 0.909 | 0.0271 |

capacitance; in one case this was obtained by a limited surface area increase from etching, and the other was a high voltage foil with relatively thick oxide dielectric.

Values of $W_{ox}/W_{in}$ were measured at either 200 V or 250 V for a larger group of commercial foils. The data are listed in Table 3. This ratio fell within a range of 0.027 to 0.054 for five different commercial etched foils with equivalent oxide thicknesses from 250 to 650 V (total of 14 specimens). The results with the lab-formed commercial type oxides on smooth substrate were within this range. There was less heat generation with the amorphous oxides, with $W_{ox}/W_{in}$ between 0.022 to 0.030.

Since pulse voltage was held in a narrow range for specimens with a wide range of oxide thicknesses, the measurements of $W_{ox}$ were obtained at different field strengths. It is likely that what we call a voltage dependence is actually a dependence of heat generation on the electric field in the dielectric. To better evaluate the results, the values of $W_{ox}/W_{in}$ were normalized to a field strength equal to half the formation field by multiplying $W_{ox}/W_{in}$ by the factor $(0.5\,V_f/V)^{n-2}$. For some combinations of foil type and $V_f$ we did not have experimental values for $n$. For those cases, the values for $n$ shown in Table 2 were used as guidelines and these values for $n$ were selected:

Foil A $V \leqslant 400$ $n = 2.43$, $V \geqslant 500$ $n = 2.0$
Foil C $V \geqslant 350$ $n = 2.0$
Foil D $450 \leqslant V \leqslant 650$ $n = 2.0$

In the last column of Table 3 are listed the normalized values of $W_{ox}/W_{in}$.

### 3.4. *Comparison of* $W_{ox}/W_{in}$ *with* $DF_{ox}$

The a.c. properties of the capacitor sandwich were measured prior to the start of each calorimetric run and the oxide *DF* was calculated from these data. The correlation between $DF_{ox}$ and the fraction of power dissipated is shown in Fig. 6. For the commercial oxides there is a dependence of heat generation on *DF*. The regression line has a slope of 2.0 and a standard deviation of 0.41. The intercept was set at (0, 0) since a dielectric with zero *DF* does not dissipate any energy. Contributions from real differences among foils, in addition to experimental error, contribute to the scatter of the data.

The cluster of data points for the two 650 $V_f$ commercial foils and the miniature capacitor are located at a heat generation rate about 50% higher than given by the regression line. The two 650 $V_f$ foils are made with different etch processes, but since they are from the same supplier, the formation processes are likely to have been the same. The relatively high

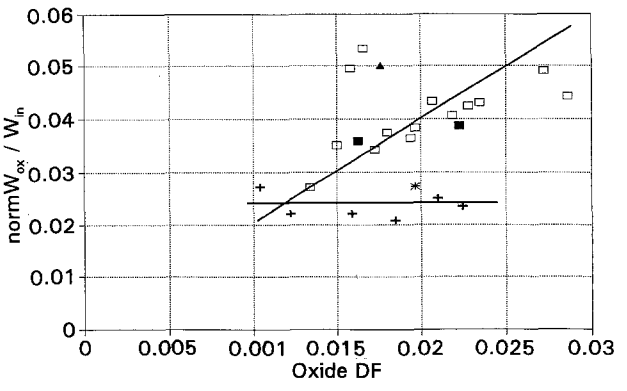


Fig. 6. Correlation of normalized heat generation with oxide *DF* for specimens listed in Table 3: (□) commercial foil and oxide; (+) commercial foil with amorphous oxide; (■) smooth foil with commercial oxide; (*) smooth foil with amorphous oxide; (▲) 400 WV capacitor.

heat generation in the capacitor will be commented on further in Section 4.

The amorphous oxides had the lowest rates of heat generation. They generate heat at a rate that is independent of oxide *DF*, over the range $0.01 < DF_{ox} < 0.023$. The average fraction of power dissipated is 0.024 with standard deviation of 0.0025. Note that the commercial foil with lowest *DF* has a heat generation rate equal to the amorphous oxide.

### 3.5. *Isothermal long term pulsing*

Up to seven million pulse cycles were applied to $300V_f$ and $350V_f$ commercial foil specimens. Pulsing at near 20° C and at 250 V produced no significant change in capacitance, and the changes in *DF* and $W_{cal}$ were small and could have been experimental variation.

Long term pulsing at a higher temperature of about 60° C produced larger changes. Capacitance change was still less than 1%, but now *DF* and $W_{cal}$ increased by significant amounts. Examples of the range of results obtained are represented by the behaviour of foil C350, previously documented in Table 2 and Fig. 5(a), and foil A500, similar to foil A275 but formed to 500 V with the lab amorphous oxide process. Sandwich capacitors were pulsed at 250 V, 50 Hz at 60° C. At intervals, *C* and *DF* were measured at 60° C and then the sandwich was removed for measurements at room temperature. Initially, and after 40–45 h of pulsing (7–8 million pulses), the sandwich was removed from the bath for measurement of $W_{cal}$. With foil C350 the experiment was continued for a total time of 122 h, about 24 million pulses. Each sandwich was then taken apart and the anode foil was reformed. Reformation means that the foil was placed in an aqueous 100 g dm$^{-3}$ boric acid solution at 70° C and 2 mA anodic current was applied until the voltage across the foil rose to $V_f$. This bath is a common solution for forming anodic barrier oxide. Foil C350 was then reassembled into a sandwich and the pulse experiment was continued.

Figure 7 shows the effect of this sequence on heat generation and oxide *DF*. The dashed lines represent

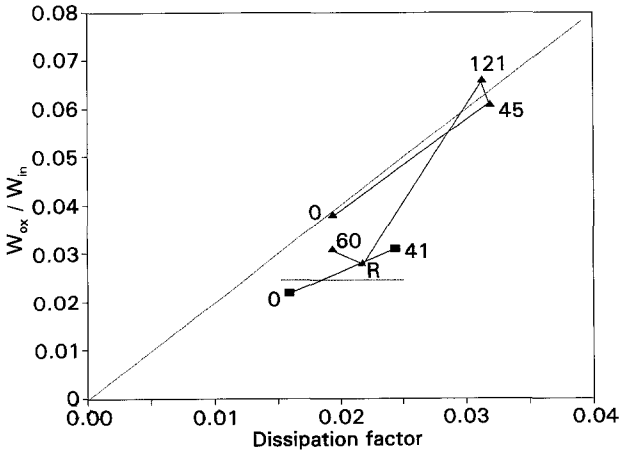


Fig. 7. Changes in heat generation and oxide *DF* during pulsing at 50 Hz, 250 V, 60° C: (▲) foil C350; (■) foil A500 amorph. See text for further description.

the correlations from Fig. 6. The number next to a data point is the pulse time, and R indicates a reformation preceding the measurement. Pulsing causes both heat generation and *DF* to increase. With foil C350 almost all of the change occurred within the initial 45 h, an additional 76 h of pulsing (121 h total) produced only a small, and perhaps not significant, increase in heat generation. Increases in $W_{ox}/W_{in}$ and *DF* from pulsing follow the same correlation as found with fresh foils. The behaviour of foil C350 is typical for the commercial oxides, but both greater and lesser changes from pulsing were observed.

Reformation of foil C350 caused a sharp reduction in both heat generation and *DF*, and further pulsing now produced only a small change in these values. The reformed values lie near those for the amorphous oxide. Note that for the A500 foil there is a modest increase in both *DF* and heat generation with pulsing. The increase in $W_{ox}/W_{in}$ is small, and we cannot tell if this represents a change from the behaviour found in the calorimeter experiments (dashed line) or is due to experimental variation.

The dependence of $DF_{ox}$ on pulse time and measuring temperature is shown in Fig. 8(a) and (b). The measurement sequence was: (i) bridge measurements at room temperature, (ii) pulsing at 60° C, (iii) bridge measurements at 60° C and (iv) sample cooled and bridge measurements at room temperature. Figure 8(a) shows $DF_{ox}$ through 45 h of pulsing. For both foils there is an increase in *DF* within the first 4 to 8 h and then *DF* varies little over the following 35 to 40 h. Considering the strong correlation between $DF_{ox}$ and heat generation, we infer that the increase in $W_{ox}/W_{in}$ first measured after 45 h pulsing is likely to have occurred during the initial 4 to 8 h. The *DF* of foil C350, when measured at 60° C is substantially higher than that measured at 20° C, whereas the amorphous oxide exhibits no such temperature dependence.

Figure 8(b) shows the measurements of foil C350 to longer times, including the reformation and subsequent pulsing. There is a slow downward trend in room temperature *DF* with pulsing. The 60° C *DF* values are scattered, but remain much higher than the room temperature values and exhibit no trend. Reformation had no discernible effect on room temperature *DF*, but the decrease in the 60° C values is most dramatic. Indeed, the 60° C *DF* is now the same as at 20° C, and the erratic behaviour is now gone. Reformation stabilized the *DF* of this foil and removed the temperature dependence, making its behaviour similar to that of the amorphous oxide.

When the reformation current was applied to the amorphous oxide, the voltage rose immediately to a stable value characteristic of the field supported by the initial formation voltage. With foil C350 the voltage initially jumped to only 245 V, and then took about 3 min to reach the formation voltage. During this interval a small amount of new oxide was deposited within the C350 dielectric layer.

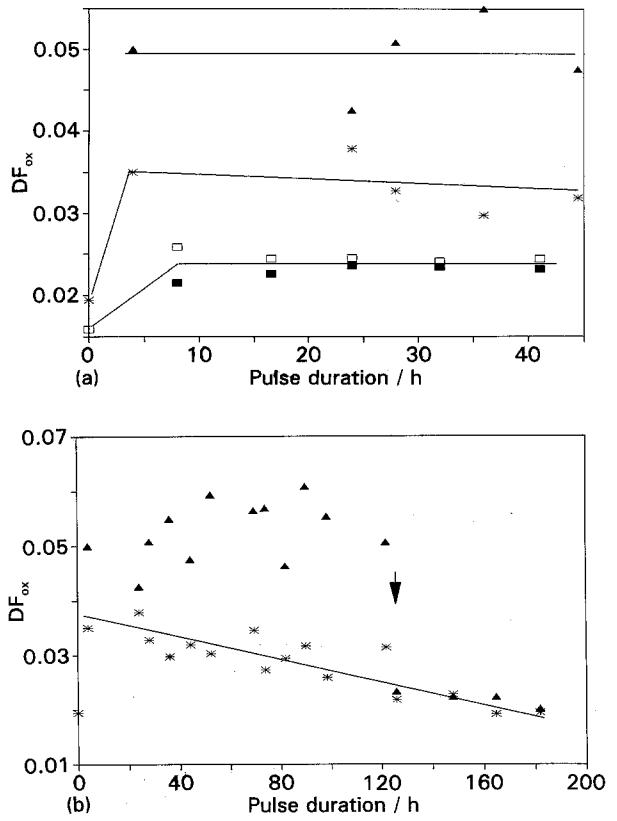


Fig. 8. (a) Oxide *DF* measured at 60° C and room temperature against duration of pulsing. Same pulse conditions and specimens as for Fig. 7. Foil and measuring temperature: foil A500, (■) 60° C and (□) *RT*; foil C350, (▲) 60° C and (*) *RT*. (b) Same as Fig. 8(a) but for longer times; foil C350 only. Arrow indicates time when foil was reformed.

## 4. Discussion

*DF* is the fraction of energy dissipated as heat during polarization by a small sinusoidal a.c. field, with energy input during both the positive and negative half-cycle. In our experiments, energy input occurs only during charging, but energy dissipation occurs during both charge and discharge. Then the minimum power dissipation expected over one complete charge + discharge cycle is $2DF$. The average value of $W_{ox}/W_{in}$ for the commercial oxides is equal to this minimum value. It appears that increasing the strength of the polarizing field did not introduce new dissipative processes with these dielectrics. With smooth foil substrates, $W_{ox} \propto V^2$, and $W_{ox}/W_{in}$ is independent of the pulse voltage. In this case, too, there appears to be no intrinsic dependence of the dissipation process on electric field, up to fields close to the growth field.

Other observations seem to be due to more complex effects of electrode structure and dielectric structure on power dissipation. A field dependence is observed with etched foil, i.e., $W_{ox}/W_{in} \propto V^n$, with $0 \leqslant n \leqslant 0.43$. The field dependent component of heat generation may arise from mechanical losses associated with the physical structure of this capacitor electrode.

It has been reported that the anodic oxide films on tantalum, niobium, and tungsten expand under the influence of an electric field [10]. No measurements have been reported for aluminium oxide, but since all these oxides grow by a high field ion conduction process and have similar dielectric properties, it is not unreasonable to expect aluminium oxide to expand upon application of a high field. From the data in [10], the strain in $Ta_2O_5$ is estimated to be about 0.004 at a field of $7 \times 10^6\,V\,cm^{-1}$, which is close to the field in an aluminium electrolytic capacitor at rated voltage. The strain depends on field as $E^m$, with $1 < m < 2$. The imposed strain is in the elastic region and the effect of field on thickness is reversible. On a flat substrate the oxide is free to expand in the direction normal to the surface. The oxide within etch tunnels is constrained in both radial and tangential directions. If a field induced strain does occur within aluminium oxide, the stress produced within an etch tunnel may be substantially greater than on a flat surface, and some frictional losses may accompany the cyclic strain from pulse operation. This may be the origin of the observed voltage dependence of heat generation.

It is difficult to explain why the amorphous oxides convert a constant fraction of input power into heat, regardless of oxide *DF* (Fig. 6). One possibility is that this is due to some porous oxide not being completely filled with barrier oxide during the second formation. Pore density is of the order $10^{20}\,cm^{-2}$ and pore size is 10–20 nm [6]. Residual porous oxide may exhibit a frequency-dependent resistance that was not distinguished from the frequency dependent barrier oxide resistance. The two factors were added for calculation of $R_{ox}$ and $DF_{ox}$, but only the barrier oxide contributes to $W_{ox}$. Although the presence of residual porous oxide is only conjecture for these specimens, in other work it has been seen to be a common occurrence.

Heat generation with commercial foils generally exceeds that with amorphous oxide (Fig. 6). The greater power dissipation in the crystalline barrier oxide is thought to be due to its specific structural features. Whereas amorphous oxide is uniform and compact [6], the crystalline barrier oxide layer tends to have microcracks and voids that are inherent to its growth process [11]. Commercial formation processes provide several stages to expose and fill the defects with anodic oxide [12]. If stabilization were not accomplished, the oxide might crack during subsequent capacitor operation, resulting in degraded dielectric properties and reduced voltage capability.

These commercial processes produce foil that is acceptably stable for most applications. The stress of long term pulsing at 60° C was sufficient to expose a small concentration of residual defects in the C350 crystalline oxide. During reformation oxide was deposited at these sites and the integrity of the dielectric was restored. No such defect structure developed during pulsing of the amorphous oxide.

It may be that cyclic mechanical forces induced by the electric field promote crack development during

pulse operation. The phenomenon has a very strong temperature dependence, since pulse operation at 60° C produces degradation of crystalline oxide within a few hours, whereas room temperature pulsing for much longer times did not cause any changes. It is significant that after reformation, *DF* and heat generation in the crystalline oxide decrease to the same levels as for the amorphous oxide (Fig. 8(b)). Thus, high heat generation does not appear to be an intrinsic property of the crystalline structure, but is associated with the defects in that layer.

It is puzzling that simply cooling the dielectric from 60° C to room temperature brings the *DF* of the crystalline oxide down to low stable values. In fact, at room temperature there is a steady decrease in *DF* with pulsing that is not at all evident at the higher measuring temperature. Whatever the cause, this temperature dependence of *DF* may be a useful diagnostic for oxide instability, since it is not displayed by the amorphous oxide nor the crystalline oxide after reformation.

The amorphous oxide had a small initial increase in *DF*, from 0.016 to 0.026 observed after 8 h pulsing at 60° C. Thus, there may be some degradation of this oxide, too, but it is clearly at a much lower level than for the crystalline oxide. There are significant differences between the behaviour observed in these experiments and that seen with the relatively large high energy density capacitors typically used for pulse discharge applications [1]. In those capacitors the heat generated is usually about 10% of the input energy. The miniature capacitor measured in the calorimeter generated 5% heat, and foils with the same *DF* produced only about 3.5% heat. There is probably a connection between these heat levels and the local temperature at the foil surface. The sandwich experiments are done on fresh foils maintained at the ambient temperature in the calorimeter. The miniature capacitor is about 1.2 cm in diameter, and it is likely that its internal temperature was above the calorimeter ambient. Note in Fig. 7 that heat generation almost doubles during pulsing of commercial foil at 60° C. Even with provision for external cooling, there is a rise in internal temperature of high energy density capacitors during pulse operation [1]. It is under such conditions that heat generation in these capacitors is measured.

A second difference is that the voltage (field) dependence of heat generation in capacitors is found to be $W_{cal} \propto V^3$ [1], a higher value of the exponent than is found in our experiments. At this time we have no data to provide an explanation, but we suggest that after degradation by pulsing the value of $n$ may increase.

A third, and most dramatic difference, is that by the simple expedient of preventing temperature increase we were able to operate the capacitor sandwiches at quite high pulse rates and pulse voltages. In a capacitor, the enhancement of oxide *DF* with increasing temperature leads to an autocatalytic situation which can terminate in runaway temperature increase. Active cooling and optimizing capacitor package design for heat rejection should result in significant improvement in pulse rate capability.

## 5. Conclusions

The fraction of input power dissipated as heat under high field pulse operation is proportional to the *DF* of the oxide dielectric for commercial aluminium anode foils. For the particular amorphous oxide used in these experiments, the heat generated was equal to the lowest obtained with commercial foils. On smooth substrates there do not appear to be any new dissipative processes introduced by pulsing at high fields. With etched foil substrates there is a field dependence of heat generation that may be due to dissipation of mechanical energy during oxide expansion and relaxation within the constraints of this particular morphology.

Long term isothermal pulsing at 60° C of commercial foils produces substantial increase in heat generation, and proportional increase in *DF* measured at 60° C. This degradation is related to voids and microcracks in the crystalline oxide dielectric and can be removed by an oxide reformation. The amorphous oxides are much more stable against degradation during pulse operation.

Little or no degradation is caused by long term pulsing at room temperature, indicating a strong temperature dependence for this process. The correlated increase in heat generation and *DF* may be sufficient to produce thermal runaway in a capacitor which has substantially greater thermal mass than the sandwiches used in these experiments.

Degraded oxides that display high *DF* at 60° C have normal *DF* when cooled to room temperature. This may be a useful diagnostic for oxide quality. It also may account for the frequent inability to identify changes in properties of foils taken from failed capacitors, because the foil measurements are usually made at room temperature.

## Acknowledgements

This work was performed for the Defense Nuclear Agency under contract DNA 001-87-C-0098, and their permission to publish is acknowledged. The contribution of Mrs Jenny Wu and Mr Scott Stillwell in obtaining the experimental data is gratefully acknowledged.

## References

[1] S. G. Parler, Jr. and J. W. Dieter, Tech. Rept. DNA-TR-90-191, Defense Nuclear Agency contract DNA 001-87-C-0098, Dec. (1991).
[2] R. S. Alwitt, *J. Electrochem. Soc.* **134** (1987) 1891.
[3] C. K. Dyer and R. S. Alwitt, *Electrochim. Acta* **23** (1978) 347.
[4] R. S. Alwitt, H. Uchi, T. R. Beck and R. C. Alkire, *J. Electrochem. Soc.* **131** (1984) 13.
[5] H. Kliem and G. Arlt, *Solid State Comm.* **59** (1986) 793;

H. Kliem and B. Schumacher, *IEEE Trans. Electr. Insul.* **EI-22** (1987) 219.
[6] H. Takahashi and M. Nagayama, *Corr. Sci.* **18** (1978) 911.
[7] C. T. Chen and G. A. Hutchins, *J. Electrochem. Soc.* **132** (1985) 1567.
[8] R. S. Alwitt, *ibid.* **114** (1967) 843.
[9] R. S. Alwitt and H. Takei, *in* 'Passivity of metals and semiconductors' (edited by M. Froment), Elsevier, Amsterdam (1984) p. 741.
[10] J. L. Ord, *J. Electrochem. Soc.* **127** (1980) 2682.
[11] R. S. Alwitt, C. K. Dyer and B. Noble, *ibid.* **129** (1982) 711.
[12] R. S. Alwitt and C. K. Dyer, *Electrochim. Acta* **23** (1978) 355.